Journal of Organometallic Chemistry 694 (2009) 4124–4133

Contents lists available at ScienceDirect

Journal of Organometallic Chemistry

journal homepage: www.elsevier.com/locate/jorganchem

Ruthenium(II)–CO complexes of N-[(2-pyridyl)methyliden]-α(or β)-aminonaphthalene: Synthesis, spectral studies, crystal structure, redox properties and DFT calculation

Papia Datta [a], Shyamal Kumar Sarkar [a], Tapan Kumar Mondal [a], Ashis Kumar Patra [b], Chittaranjan Sinha [a,*]

[a] Department of Chemistry, Inorganic Chemistry Section, Jadavpur University, Kolkata 700032, India
[b] Inorganic and Physical Chemistry Department, Indian Institute of Science, Bangalore, India

ARTICLE INFO

Article history:
Received 2 September 2008
Received in revised form 9 September 2009
Accepted 14 September 2009
Available online 17 September 2009

Keywords:
Schiff bases
Ruthenium–carbonyl
X-ray structure
DFT and TD-DFT computation
Luminescence

ABSTRACT

The characterization and properties of *trans*-(X)-[$RuX_2(CO)_2$(α/β-NaiPy)] (**1**, **2**) (α-NaiPy (**a**), β-NaiPy (**b**); X = Cl (**1**), I (**2**)) are described in this work. The structures are confirmed by single crystal X-ray diffraction studies. Reaction of these compounds with Me_3NO in MeCN has isolated monocarbonyl *trans*-(X)-[RuX_2-(CO)(MeCN)(α/β-NaiPy)] (**3**, **4**). The complexes show intense emission properties. Quantum yields of **1** and **2** (ϕ = 0.02–0.08) are higher than **3** and **4** (ϕ = 0.006–0.015). Voltammogram shows higher Ru(III)/Ru(II) (1.3–1.5 V) potential of **1** and **2** than that of **3** and **4** (0.8–0.9 V) that may be due to coordination of two π-acidic CO groups in former. The electronic spectra and redox properties of the complexes are compared with the results obtained by density functional theory (DFT) and time-dependent density functional theory (TD-DFT) using polarizable continuum model (CPCM).

1. Introduction

2.2′-Bipyridine is one of the most popular bidentate N,N-chelating agent, so far used, in the development of coordination chemistry of heterocyclic nitrogenous ligand [1,2]. These complexes display exciting photochemical and photophysical properties, and have been applied in many technological fields [3]. Their luminescent properties have also found applications in solar energy converters [4], in electroluminescent systems [5], and, particularly, in probes and sensors [6]. They have been applied in electron transfer processes [7,8] and as catalyst and stoichiometric redox reagents [9]. This has aroused immense interest to modify the ligand structure [7,10] by other heterocycle, changing ring size, adding substituents and different hetero atoms in the ring, incorporating other functional groups, molecular parts, etc.

Functional property of polypyridine is due to π-acidic diimine chelation (–N=C–C=N–) [7]. In the synthesis of new ligands imino-pyridine has been attracted in the last few years [11]. They are derived from the condensation of pyridine-2-carboxaldehyde and (aliphatic/aromatic) primary amine. Furthermore, mixed ligand complexes with polypyridine and carbonyls have been investigated as potential catalyst for water–gas shift reaction [12], CO_2 reduction, and hydroformylation reaction of alkenes in 1980s [13]. [$Ru(bpy)(CO)_2Cl_2$] is an excellent catalyst for the photochemical and electrochemical reduction of CO_2 into formate [14]. Besides, ruthenium–carbonyl complexes are very recently used as CORM (*carbon monoxide releasing molecules*) those liberate CO to elicit direct biological activities such as, anti-inflammatory and anti-apoptotic properties, promotes cardioprotection [15]. Since then a renewed impetus has been given to design and explore ruthenium–carbonyl–polypyridine complexes.

This work is addressed to ruthenium-carbonyl complexes of Schiff bases, N-[(2-pyridyl)methyliden]-α(or β)-aminonaphthalene (α/β-NaiPy). The ligand has been synthesized from the condensation of naphthylamines and pyridine-2-carboxaldehyde. There are few reports on the chemistry of α/β-NaiPy [16–19]. Naphthyl group is sterically more crowded, electronically labile and more delocalized than phenyl group. Thus, naphthyl substituent in Schiff base may affect significantly the spectroscopic and photophysical properties of metal complexes compared to the properties of phenyl Schiff bases. Herein we wish to report the synthesis, spectral characterization, structure, electrochemistry and luminescence properties of *trans*-(X)-[$RuX_2(CO)_2${N-[(2-pyridyl)methyliden]-α(or β)-aminonaphthalene (α or β-NaiPy)}] (X = Cl, I). DFT and TD-DFT calculation of optimized geometry has been used to explain spectral and redox properties.

* Corresponding author.
E-mail address: c_r_sinha@yahoo.com (C. Sinha).

0022-328X/$ - see front matter © 2009 Elsevier B.V. All rights reserved.
doi:10.1016/j.jorganchem.2009.09.017

2. Experimental

2.1. Materials and measurements

α-Naphthylamine and β-naphthylamine were purchased from Thomas Baker & Co. Pyridine-2-carboxaldehyde was purchased from Lancaster Ltd., England. N-[(2-pyridyl)methyliden]-α(or β)-aminonaphthalene (α or β-NaiPy) were synthesized by equimolar condensation of pyridine-2-carboxaldehyde and naphthylamine in ethanol [16].

$[Ru(CO)_2Cl_2]_n$ was synthesized by published procedure [20]. Reactions were carried out under extremely dry oxygen free atmosphere under Atmos bags (Sigma–Aldrich). All other chemicals used were of A.R. quality and were used as received from SRL, India.

For the solution spectral studies spectroscopic grade solvents were used from Lancester, UK. Microanalyses (C, H, N) were performed using a Perkin–Elmer 2400 CHN elemental analyzer. Spectroscopic measurements were carried out using the following instruments: UV–vis spectra, Lambda 25 Perkin Elmer; FT-IR spectra (KBr disk), RX-1 Perkin Elmer; ^{1}H NMR and ^{13}C NMR spectra in $CDCl_3$ Bruker 300 MHz FT-NMR spectrometers in presence of TMS as internal standard. Luminescence property was measured using LS-55 Perkin Elmer fluorescence spectrophotometer at room temperature (298 K) in acetonitrile solution by 1 cm path length quartz cell. Fluorescence lifetimes were measured using a time-resolved spectrofluorometer from IBH, UK. The instrument uses a picosecond diode laser (NanoLed-03, 370 nm) as the excitation source and works on the principle of time-correlated single photon counting [21]. The instrument functions ~230 ps at FWHM. To eliminate depolarization effects on the fluorescence decays, measurements were done with magic angle geometry (54.7°) for the excitation and emission polarizers. The goodness of fit was evaluated by ø2 criterion and visual inspection of the residuals of the fitted function to the data. The lifetimes were measured in air-equilibrated solution at ambient temperature. FAB-MS was collected from JEOL-JMS 600. Electrochemical measurements were carried out with the use of computer controlled EG & G PARC VersaStat model 250 Electrochemical instrument using a Pt-disk working electrode and Pt-wire auxiliary electrode under inert (dry N_2) environment in CH_3CN. The solution was IR compensated and the results were collected at 298 K. The reported results were referenced to Ag/AgCl in CH_3CN and were uncorrected for junction potential. [n-Bu_4N]-[ClO_4] was used as supporting electrolyte.

The fluorescence quantum yield of the complexes was determined using carbazole and phenanthrene as references with a known ϕ_R of 0.42 and 0.13 respectively in MeCN. The complex and the reference dye were excited at the same wavelength, maintaining nearly equal absorbance (~0.1), and the emission spectra were recorded. The area of the emission spectrum was integrated using the software available in the instrument and the quantum yield is calculated according to the following equation:

$$\phi_S/\phi_R = [A_S/A_R] \times [(Abs)_R/(Abs)_S] \times [\eta_S^2/\eta_R^2]$$

Here, ϕ_S and ϕ_R are the fluorescence quantum yield of the sample and reference, respectively. A_S and A_R are the area under the fluorescence spectra of the sample and the reference respectively, $(Abs)_S$ and $(Abs)_R$ are the respective optical densities of the sample and the reference solution at the wavelength of excitation, and η_S and η_R are the values of refractive index for the respective solvent used for the sample and reference.

2.1.1. Preparation of [$RuCl_2(CO)_2$(α-NaiPy)] (**1a**)

To $[Ru(CO)_2Cl_2]_n$ (50 mg, 0.219 mmol) dissolved in dry acetonitrile (15 cm^3) α-NaiPy (51 mg, 0.22 mmol) was added and the solution was refluxed for 5 h. The color of the solution changed to deep brown red. Then the solvent was evaporated under low pressure and the crude product was chromatographed in a neutral Al_2O_3 column prepared in petroleum-ether (60–80° fraction). A red portion was eluted with 1:2 (v/v) acetonitrile–benzene. Removal of the solvent afforded analytically pure product [$RuCl_2(CO)_2$(α-NaiPy)] in 65% yield.

Microanalytical data are as follows: Anal. Calc. for [$RuCl_2(CO)_2$(α-NaiPy)] (**1a**), $C_{18}H_{12}N_2O_2Cl_2Ru$, C, 46.96; H, 2.61; N, 6.09. Found: C, 46.91; H, 2.64: N, 6.11%. FAB-MS, m/z = 460 (M^+), 432 ($M-CO)^+$, 404 ($M-2CO)^+$; IR (KBr, cm^{-1}) ν_{CO}, 2059, 1990 cm^{-1}.

Reaction of $[Ru(CO)_2Cl_2]_n$ with β-NaiPy has synthesised the complex [$RuCl_2(CO)_2$(β-NaiPy)] (**1b**) (yield 60%; brown red).

Microanalytical data are as follows: Anal. Calc. for [$RuCl_2(CO)_2$(β-NaiPy)] (**1b**), $C_{18}H_{12}N_2O_2Cl_2Ru$, C, 46.96; H, 2.61; N, 6.09. Found: C, 46.88; H, 2.62: N, 6.13%. FAB-MS, m/z = 460 (M^+), 432 ($M-CO)^+$, 404 ($M-2CO)^+$; IR (KBr, cm^{-1}) ν_{CO}, 2063, 1999 cm^{-1}.

2.1.2. Synthesis of [$Ru(CO)_4I_2$]

$Ru_3(CO)_{12}$ (500 mg; 0.68 mmol) and I_2 (199 mg; 0.78 mmol) were taken in 1:3 molar ratio in a mortar and finely mixed. The mixture was then transferred in a Teflon reactor in hexane, corked and placed in the microwave oven 450 W for 5 min with 5 min interval between each step. Seven steps were performed cyclically. A brown residue of $Ru(CO)_4I_2$ was obtained. The mixture was then filtered and washed with n-hexane.

Microanalytical data are Anal. Calc. for $Ru(CO)_4I_2$: $C_4O_4I_2Ru$, C, 10.26. Found: C, 10.25%. FAB-MS, m/z = 467 (M^+), 439 ($M-CO)^+$, 411 ($M-2CO)^+$, etc.; IR (KBr, cm^{-1}) ν_{CO}, 2011, 2059, 2118 cm^{-1}.

2.1.3. Synthesis of [$RuI_2(CO)_2$(α/β-NaiPy)] (**2**)

To an acetonitrile solution of [$Ru(CO)_4I_2$] (100 mg; 0.21 mmol)α-NaiPy /β-NaiPy (149.7 mg, 0.21 mmol) was added and refluxed for 5 h under dry dinitrogen. The dark red solid product was obtained by the evaporation of the solvent. The compound was then purified by previously described chromatographic process. The yield was 70%.

Microanalytical data are as follows: Anal. Calc. for [$RuI_2(CO)_2$(α-NaiPy)] (**2a**), $C_{16}H_{12}N_2O_2I_2Ru$, C, 29.86; H, 1.87; N, 4.35. Found: C, 29.89; H, 1.90: N, 4.31%. FAB-MS, m/z = 643 (M^+), 615 ($M-CO)^+$, 587 ($M-2CO)^+$; IR (KBr, cm^{-1}) ν_{CO}, 2047, 1985 cm^{-1}. [$RuI_2(CO)_2$(β-NaiPy)] (**2b**), $C_{16}H_{12}N_2O_2I_2Ru$, C, 29.86; H, 1.87; N, 4.35%; Found: C, 29.85; H, 1.82: N, 4.38%. FAB-MS, m/z = 643 (M^+), 615 ($M-CO)^+$, 587 ($M-2CO)^+$; IR (KBr, cm^{-1}) ν_{CO}, 2048, 1971 cm^{-1}.

2.1.4. Preparation of [$RuCl_2(CO)(CH_3CN)$(α-NaiPy)] (**3a**)

To a solution of [$RuCl_2(CO)_2$(α/β-NaiPy)] (80 mg, 0.293 mmol) in dry acetonitrile (20 cm^3) was added Me_3NO (25 mg, 0.294 mmol) and the resulting solution was refluxed for 2 h under nitrogen atmosphere. The color of the solution changed from brown red to purple. The solvent was then evaporated after cooling to room temperature. The remaining mixture was redissolved in dichloromethane and purified by chromatography on a neutral alumina column prepared in petroleum–ether (60–80° fractions). A purple red solution was eluted with 1:1 (v/v) acetonitrile–benzene. The solution was then evaporated to dryness which yielded analytically pure product [$RuCl_2(CO)(CH_3CN)$(α-NaiPy)] in 45% yield.

Microanalytical data are as follows: Anal. Calc. for [$RuCl_2(CO)(CH_3CN)$(α-NaiPy)] (**3a**), $C_{19}H_{15}N_3OCl_2Ru$, C, 48.20; H, 3.17; N, 8.88. Found: C, 48.18; H, 3.16: N, 8.83%. FAB-MS, m/z = 473 (M^+), 445 ($M-CO)^+$; IR (KBr, cm^{-1}) ν_{CO}, 1968 cm^{-1}.

Microanalytical data are as follows: Anal. Calc. for [$RuCl_2(CO)(CH_3CN)$(β-NaiPy)] (**3b**), $C_{19}H_{15}N_3OCl_2Ru$, C, 48.20; H, 3.17; N, 8.88. Found: C, 48.23; H, 3.19: N, 8.89%. FAB-MS, m/z = 473 (M^+), 445($M-CO)^+$; IR (KBr, cm^{-1}) ν_{CO}, 1970 cm^{-1}.

Reaction of $[RuI_2(CO)_2(\alpha/\beta\text{-NaiPy})]$ (**2**) with Me_3NO in MeCN under identical condition has afforded the complex $[RuI_2(CO)(CH_3CN)(\alpha/\beta\text{-NaiPy})]$ (yield 55%; purple red).

Microanalytical data are as follows: Anal. Calc. for $[RuI_2(CO)(CH_3CN)(\alpha\text{-NaiPy})]$ (**4a**), $C_{19}H_{15}N_3OI_2Ru$, C, 34.76; H, 2.29; N, 6.40. Found: C, 34.85; H, 2.25: N, 6.25%. FAB-MS, $m/z = 656$ (M^+), 628 ($M-CO)^+$; IR (KBr, cm^{-1}) ν_{CO}, 1960 cm^{-1}.

Microanalytical data are as follows: Anal. Calc. for $[RuI_2(CO)(CH_3CN)(\beta\text{-NaiPy})]$ (**4b**), $C_{19}H_{15}N_3OI_2Ru$, C, 34.76; H, 2.29; N, 6.40. Found: C, 34.87; H, 2.31: N, 6.33%. FAB-MS, $m/z = 656$ (M^+), 628 ($M-CO)^+$; IR (KBr, cm^{-1}) ν_{CO}, 1962 cm^{-1}.

2.2. X-Ray diffraction study of $[RuCl_2(CO)_2(\beta\text{-NaiPy})]$ (**1b**)

The crystallographic data are shown in Table 1. A suitable single crystal of $[RuCl_2(CO)_2(\beta\text{-NaiPy})]$ (**1b**) ($0.70 \times 0.23 \times 0.13$ mm) was mounted on a CCD Diffractometer equipped with fine-focus sealed tube graphite monochromated Mo Kα ($\lambda = 0.71073$ Å) radiation. The unit cell parameters and crystal-orientation matrices were determined by least squares refinements of all reflections. The intensity data were corrected for Lorentz and polarization effects and an empirical absorption correction were also employed using the Bruker SAINT program [22]. Data were collected applying the condition $I > 2\sigma(I)$. Out of total 13 135 data 3487 were used within *hkl* parameters $-15 \leqslant h \leqslant 17$; $-10 \leqslant k \leqslant 10$; $-22 \leqslant l \leqslant 22$ for structure solution. All these structures were solved by direct methods and followed by successive Fourier and difference Fourier syntheses. Full matrix least squares refinements on F^2 were carried out using SHELXL-97 with anisotropic displacement parameters for all non-hydrogen atoms. Hydrogen atoms were constrained to ride on the respective carbon or nitrogen atoms with isotropic displacement parameters equal to 1.2 times the equivalent isotropic displacement of their parent atom in all cases of aromatic units. All calculations were carried out using SHELXS 97 [23], SHELXL 97 [24], PLATON 99 [25] and ORTEP [26] programs.

Table 1
Selected crystallographic data for *trans*-(Cl)-$[RuCl_2(CO)_2(\beta\text{-NaiPy})]$ (**1b**).

	$[RuCl_2(CO)_2(\beta\text{-NaiPy})]$
Formula	$C_{18}H_{12}Cl_2N_2O_2Ru$
Crystal size (mm^3)	$0.70 \times 0.23 \times 0.13$
Formula weight ($g\ M^{-1}$)	460.27
Crystal system	monoclinic
Space group	$P2_1/c$ (No. 14)
a (Å)	14.241(5)
b (Å)	8.645(3)
c (Å)	17.872(5)
α (°)	90.0
β (°)	125.917(19)
γ (°)	90.0
V ($Å^3$)	1782.0(10)
Z	4
T (K)	293(2)
Density (calculated) (Mg/m^3)	1.716
λ (Å) (Mo Kα)	0.71073
Absorption coefficient (mm^{-1})	1.193
Data/restraints/parameters	3487/8/226
Goodness-of-fit on F^2	1.007
$R(F_o)$[a] $[I > 2\sigma(I)]$	0.0650
$wR(F_o)$[b] $[I > 2\sigma(I)]$	0.1186
R [all data] (wR [all data])	0.1322 (0.1438)
Largest difference in peak and hole (e $Å^{-3}$)	0.629, −0.435
Weight factor: $w = 1/[\sigma^2(F_o^2) + (AP)^2 + (BP)]$	$A = 0.0626$; $B = 1.447$

[a] $R = \sum||F_o| - |F_c||/\sum|F_o|$.
[b] $wR = \{\sum[w(F_o^2 - F_c^2)^2]/\sum[w(F_o^2)^2]\}^{1/2}$; $w = [\sigma^2(F_o)^2 + (AP)^2 + BP]^{-1}$, where $P = (F_o^2 + 2F_c^2)/3$.

2.3. DFT and TD-DFT calculations

Full geometry optimizations were carried out using the density functional theory method at the (R)B3LYP level for **1b** and **2b** [27]. The 6-311G(d) basis set was used for C, H, N and O atoms while Stuttgart/Dresden SDD basis set with effective core potential was employed for iodine and ruthenium atoms [28]. The vibrational frequency calculations were performed to ensure that the optimized geometries represent the local minima and there are only positive eigen values. All calculations were performed with GAUSSIAN03 program package [29] with the aid of the GAUSSVIEW visualization program [30]. Vertical electronic excitations based on B3LYP optimized geometries was computed using the time-dependent density functional theory (TD-DFT) formalism [31] in acetonitrile using conductor-like polarizable continuum model (CPCM) [32]. GaussSum [33] was used to calculate the fractional contributions of various groups to each molecular orbital.

3. Results and discussion

3.1. Synthesis and formulation

The reaction of α/β-NaiPy and $[Ru(CO)_2Cl_2]_n/[Ru(CO)_4I_2]$ under stirring and refluxing condition in dry MeCN under N_2 environment for a period of 5 h has synthesized brown red complexes in 60–70% yield (Eqs. (1) and (2)). The ligands, N-[((2-pyridyl)methyliden)-α/β-aminonaphthalene] (α-NaiPy (**a**), β-NaiPy (**b**)) are N,N′-chelating system where N and N′ refer to N(pyridyl) and N(imine) donor centers, respectively (Scheme 1). The composition of the complexes, $[RuX_2(CO)_2(NaiPy)]$ (X = Cl (**1**), I (**2**)) has been supported by microanalytical and spectroscopic data. Three isomers *trans*-(X)-$[RuX_2(CO)_2(N,N')]$ (**1, 2**), *cis*-(X)-$[RuX_2(CO)_2(N,N')]$ (**1′**, **2′**), *cis*-(CO, X)-$[RuX_2(CO)_2(N,N')]$ (**1″**/**2″**) are possible. However, we have isolated only one isomer: CO groups are in *cis* (**1** and **2**) and two X are in *trans* disposition (Scheme 1). The complexes are diamagnetic, indicating the presence of metal in the +2 oxidation state (d^6)

$$[Ru(CO)_2(Cl)_2]_n + \text{NaiPy} \xrightarrow[\text{Nitrogen atmosphere}]{\text{Reflux for 5 h in MeCN}} \textit{trans}\text{-(Cl)-}[RuCl_2(CO)_2(\text{NaiPy})] \quad (1)$$

$$[Ru(CO)_2(I)_2]_n + \text{NaiPy} \xrightarrow[\text{Nitrogen atmosphere}]{\text{Reflux for 5 h in MeCN}} \textit{trans}\text{-(I)-}[RuI_2(CO)_2(\text{NaiPy})] \quad (2)$$

$$\textit{trans}\text{-(X)-}[RuX_2(CO)_2(\text{NaiPy})] \xrightarrow{\text{Excess } Me_3No} \textit{trans}\text{-(X)-}[RuX_2(CO)_2(\text{NaiPy})(\text{NCMe})] \quad (3)$$

The structure has been established by single crystal X-ray diffraction study in case of $[RuCl_2(CO)_2(\beta\text{-NaiPy})]$ (**1b**) and has *trans*-(Cl) geometry. The higher stability of *trans*-(Cl)-*cis*-(CO) isomer relative to *cis*-(Cl)-*trans*-(CO) is also known in analogous 1-alkyl-2-(arylazo)imidazole complexes of ruthenium(II) [33] which is not surprising due to the *trans* weakening effect of CO. The selectivity of *trans*-(Cl) configuration has also been supported by DFT calculations (*vide DFT section*). The complexes, **1** and **2** undergo selective monodecarbonylation reaction upon refluxing with Me_3NO in acetonitrile (Eq. (3)) and has synthesised, *trans*-(Cl)-$[RuCl_2(CO)(MeCN)(\alpha/\beta\text{-NaiPy})]$ (**3**), *trans*-(I)-$[RuI_2(CO)(MeCN)(\alpha/\beta\text{-NaiPy})]$ (**4**). Considering structure of precursor (**1** and **2**) we may assume the configuration of **3** and **4** as *trans*-(Cl)-$[RuCl_2(CO)(MeCN)(NaiPy)]$. Photochemical treatment of *trans*-(X)-$[RuCl_2(CO)_2(\alpha/\beta\text{-NaiPy})]$ is unsuccessful to isomerise and to decarbonylate completely. Rather light irradiation in MeCN solution has synthesized monocarbonyl compounds *trans*-(X)-$[RuX_2(CO)(MeCN)(\alpha/\beta\text{-NaiPy})]$. The crystals of these complexes are weakly diffracting for X-ray structure determination. Complete

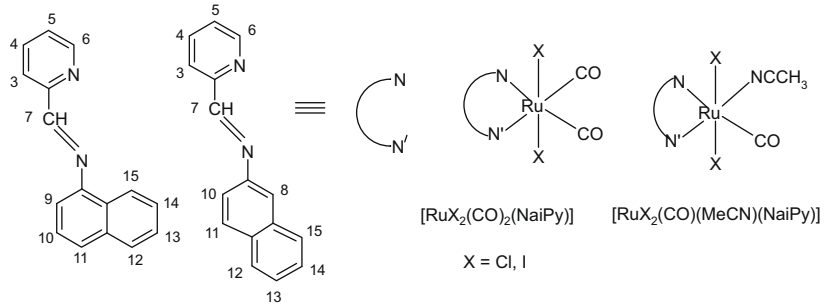

[$RuCl_2(CO)_2$(α-NaiPy)] (**1a**), [$RuCl_2(CO)_2$(β-NaiPy)] (**1b**), [$RuI_2(CO)_2$(α-NaiPy)] (**2a**), [$RuI_2(CO)_2$(β-NaiPy)] (**2b**), [$RuCl_2(CO)(CH_3CN)$(α-NaiPy)] (**3a**), [$RuCl_2(CO)(CH_3CN)$(β-NaiPy)] (**3b**), [$RuI_2(CO)(CH_3CN)$(α-NaiPy)] (**4a**), [$RuI_2(CO)(CH_3CN)$(β-NaiPy)] (**4b**)

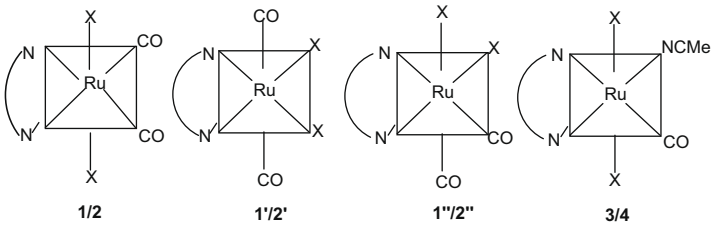

Scheme 1.

removal of CO has not been achieved even under drastic reaction condition in presence of large excess of Me_3NO. This reaction has yielded an intractable brown solid. All these complexes are diamagnetic which indicates that ruthenium is in divalent state (Ru(II)).

3.2. Molecular structure

The X-ray structure of *trans*-(Cl)-[$RuCl_2(CO)_2$(β-NaiPy)] (**1b**) is shown in Fig. 1; selected bond parameters are listed in Table 2.

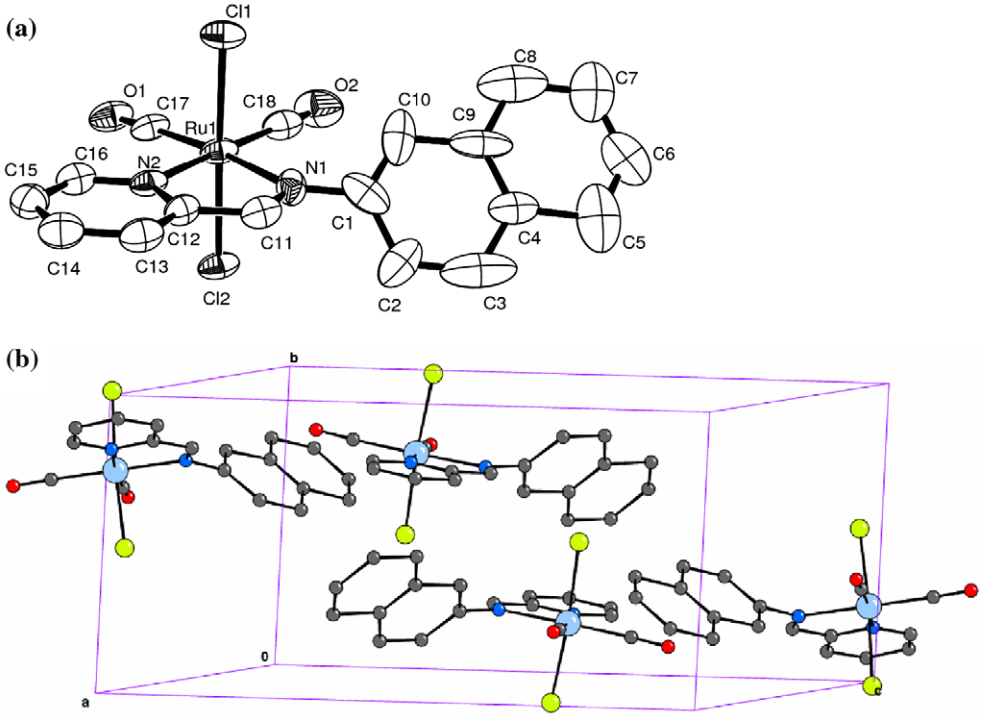

Fig. 1. (a) Molecular structure of *trans*-(Cl)-[$RuCl_2(CO)_2$(β-NaiPy)] (**1b**) and (b) unit cell packing diagram.

Table 2
Selected bond lengths (Å) and angles (°) for the complex *trans*-(Cl)-[$RuCl_2(CO)_2$(β-NaiPy)] (**1b**) with estimated standard deviations in the parentheses.

Bond distances (Å)	Experimental	Calculated	Bond angle (°)	Experimental	Calculated
Ru(1)–N(1)	2.120(6)	2.155	N(1)–Ru(1)–N(2)	76.3(2)	76.83
Ru(1)–N(2)	2.130(6)	2.150	N(1)–Ru(1)–Cl(1)	88.39(16)	85.07
Ru(1)–C(17)	1.890(9)	1.883	N(1)–Ru(1)–Cl(2)	86.56(16)	92.96
Ru(1)–C(18)	1.867(11)	1.910	N(1)–Ru(1)–C(17)	172.0(3)	172.3
Ru(1)–Cl(1)	2.374(2)	2.445	N(1)–Ru(1)–C(18)	100.0(3)	96.45
Ru(1)–Cl(2)	2.3768(19)	2.457	N(2)–Ru(1)–Cl(1)	87.98(14)	87.80
C(17)–O(1)	1.111(8)	1.150	N(2)–Ru(1)–Cl(2)	88.69(14)	85.39
C(18)–O(2)	1.130(9)	1.148	N(2)–Ru(1)–C(17)	96.1(3)	96.47
			N(2)–Ru(1)–C(18)		92.52
			C(17)–Ru(1)–C(18)	87.7(4)	90.29
			C(17)–Ru(1)–Cl(1)	93.8(2)	90.98
			C(17)–Ru(1)–Cl(2)	90.9(2)	90.19
			C(18)–Ru(1)–Cl(1)	91.2(2)	92.55
			C(18)–Ru(1)–Cl(2)	91.9(2)	94.16
			Cl(1)–Ru(1)–Cl(2)	174.49(7)	173.2

The molecule consists of a central Ru surrounded by six donor centers, and the arrangement is distorted octahedral. The atomic arrangement involves two *trans*-chlorine, two *cis*-CO and chelated β-NaiPy within the $RuCl_2C_2N_2$ coordination sphere. The *trans*-chlorine angle, Cl(1)–Ru(1)–Cl(2) is 174.49 (7)°. Other angles about Ru define the distorted octahedral geometry.

The Ru–N(imine), [Ru(1)–N(1), 2.120(6) Å], is slightly shorter than Ru–N(pyridine) (Ru(1)–N(2), 2.130(6) Å). In the Ru–C bond lengths (Ru(1)–C(17), 1.890(9); Ru(1)–C(18), 1.867(11) Å) the bonds *trans* to Ru–N(pyridine) (Ru(1)–C(18)) is shorter than the bonds those are *trans* to Ru–N(imine) (Ru(1)–C(17)). That may be due to higher π-acidity of pyridine-N than exocyclic imine-N. The C–O distances differ significantly; C(18)–O(2) (1.130(9) Å) is elongated by ~0.02 Å than C(17)–O(1), (1.111(8) Å). The bond lengths and angles are comparable with the parameters of [$RuCl_2$-$(CO)_2$(bpy)] [34] and. [$RuCl_2(CO)_2$(HaaiEt)] (HaaiEt = 1-ethyl-2-(phenylazo)imidazole) [35].

The calculated structure of **1b** correlates well with the results of its X-ray analysis (Fig. 1, Table 2). The theoretical Ru-N bond lengths are about 0.02–0.03 Å longer than that of observed one. The experimental Ru–Cl distances are shortened by 0.07–0.08 Å than theoretical data. The Ru–C and C–O distances are also reduced by 0.04–0.07 Å and 0.01–0.04 Å, respectively, in the experimental than calculated structure.

The reason of isolation of **1b** isomer may be answered from DFT calculation. It shows that energy of HOMO of *trans*-(Cl)-[$RuCl_2$-$(CO)_2$(β-NaiPy)] (**1b**) is −6.08 eV and that of *cis*-(Cl)-[$RuCl_2$-$(CO)_2$(β-NaiPy)] and *cis*-(Cl, CO)-[$RuCl_2(CO)_2$(β-NaiPy)] are −5.92 and −6.32 eV, respectively. The results show that *cis*-(Cl, CO) has lowest energy. It is the experimental condition that may be appropriate to populate next level and thus *trans*-(Cl)-[$RuCl_2$-$(CO)_2$(β-NaiPy)] (**1b**) is isolated. The energy of HOMO of *trans*-(I)-[$RuI_2(CO)_2$-(β-NaiPy)] (**2b**) (E_{HOMO}: −5.83 eV) is higher than the *trans*-(Cl)-[$RuCl_2(CO)_2$(β-NaiPy)] (**1b**) (E_{HOMO}: −6.00 eV) which suggests better stability of the chloride complex than the iodide one. The electronegativity difference of Cl and I may cause higher stability of **1b** than **2b**.

3.3. Spectroscopic characterization

3.3.1. FT-IR and mass spectra

The infrared spectra of **1** and **2** show the presence of two ν(CO) stretching vibrations at 1971–1999 and 2047–2063 cm^{-1} which indicate the *cis* coordination of two COs [20,36]. Usually ν(CO) of **1** appear at higher frequency than **2**. The ν(Ru–Cl) of **1** appears at 330–340 cm^{-1}. We can not detect ν(Ru–I) for the complexes **2** as we can not scan FT-IR beyond 200 cm^{-1} (Section 2). However, the effect of Ru–I in **2** is observed by decreasing ν(CO) relative to **1**. Other significant peaks appear at 1590–1630 cm^{-1} correspond to ν(C=N). The ν(C=N) is significantly shifted to lower frequency region (1580–1600 cm^{-1}) compared to free ligand value (1590–1620 cm^{-1}) [37] which supports efficient back donation, d π(Ru(II)) → π*(imine). The infrared spectra of **3** and **4** show one ν(CO) at 1960–1970 cm^{-1} and is in support of monocarbonyl formulation [34,35] and shifting at lower frequency region compared to ν(CO) of **1** and **2**, respectively, is an indication of better d π(Ru(II)) → π*(CO) in **3** and **4**. The molecular ion peak as well as the peaks obtained at mass values $(M-CO)^+$, $(M-2CO)^+$ for **1** and **2** and at $(M-CO)^+$ for **3** and **4** by FAB-MS supports the formation of the expected monocarbonyl complex.

3.3.2. UV–Vis and emission spectra

The electronic spectra of the complexes, show a broad low intense band ($\varepsilon \sim 600$–$1800\ M^{-1}\ cm^{-1}$) at 500–530 nm in addition to high intense bands at 340–410 nm (Fig. 2, Table 3). Free ligands **a** and **b** show intense transitions at 258, 275–288 and 300–344 nm. The shorter wavelength transitions are ligand centered (n–π* and π–π*) transitions. DFT and TD-DFT calculations are used to explain the origin of transitions.

The DFT calculations have been done using optimized geometry of representative complexes of the series [$RuX_2(CO)_2$(β-NaiPy)] (X = Cl (**1b**), I (**2b**)). The HOMO and HOMO-1 of *trans*-(Cl)-[$RuCl_2$-

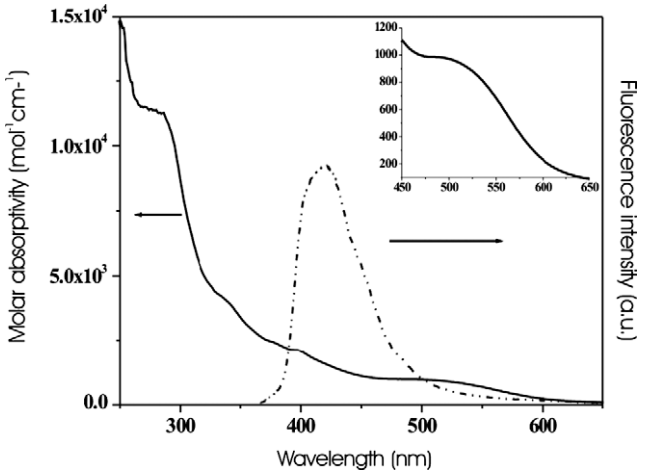

Fig. 2. Electronic absorption and emission spectra of [$RuCl_2(CO)_2$(α-NaiPy)] (**1a**). Inset picture shows absorption spectra of **1a** at higher wavelength.

Table 3
Cyclic voltammetry[b], absorption[a], fluorescence[a] spectra and lifetime[a] data.

Compound	Cyclic voltammetric data[b]		Absorption[a] λ_{max} (nm) ($10^{-3}\varepsilon$ [M^{-1} cm^{-1}])	$\lambda_{max(Excitation)}$ (nm)	$\lambda_{max(Emission)}$ (nm)	Quantum yield (φ)	Lifetime (τ) (ns)	(χ^2)	$k_r \times 10^{-9}$ (s^{-1})	$k_{nr} \times 10^{-9}$(s^{-1})
	E_M (V) (ΔE_p, mV)	E_L (V) (ΔE_p, mV)								
[$RuCl_2(CO)_2$ (α-NaiPy)] (1a)	1.48 (190)	−1.28 (220)	286 (11.236), 342 (3.906), 399 (2.103), 512 (0.941)	342	414	0.082	1.253	0.98	0.065	0.733
[$RuCl_2(CO)_2$ (β-NaiPy)] (**1b**)	1.45 (230)	−1.19 (260)	328 (3.667), 383 (1.906), 520 (0.748)	328	426	0.046	1.143	0.83	0.012	0.875
[$RuI_2(CO)_2$ (α-NaiPy)] (**2a**)	1.34 (195)	−1.25 (215)	229 (47.76), 309 (20.52), 402(4.86), 521 (0.60)	309	407	0.037	1.193	1.08	0.0310	0.807
[$RuI_2(CO)_2$ (β-NaiPy)] (**2b**)	1.32 (198)	−1.22 (190)	229 (27.99), 305 (8.87), 407 (2.90), 524(0.65)	305	354	0.024	1.045	1.1	0.0134	0.944
[$RuCl_2(CO)(CH_3CN)$ (α-NaiPy)] (**3a**)	0.909 (225)	−1.20 (230)	282 (9.424), 346 (2.668), 399 (1.587), 515 (1.242)	346	424	0.0152	1.096	1.02	0.014	0.898
[$RuCl_2(CO)(CH_3CN)$ (β-NaiPy)] (**3b**)	0.879 (280)	−1.18 (270)	275 (15.096), 318 (7.094), 368 (3.825), 502 (1.759),	318	415	0.011	0.906	0.96	0.0017	1.102
[$RuI_2(CO)(CH_3CN)$ (α-NaiPy)] (**4a**)	0.852 (208)	−1.15 (210)	261 (22.03), 300 (11.39), 405 (2.92), 503 (1.11)	300	434	0.010	1.003	0.95	0.010	0.987
[$RuI_2(CO)(CH_3CN)$ (β-NaiPy)] (**4b**)	0.810 (210)	−1.14 (200)	230 (56.59), 291 (20.88), 397 (7.14), 508 (0.65)	291	354	0.006	0.876	0.99	0.0068	1.135

[a] Solvent, MeCN.
[b] Solvent, MeCN Pt-working electrode, Ag/AgCl reference Electrode, Pt-auxiliary electrode; [n-Bu_4N](ClO_4) supporting electrolyte, scan rate 50 mV/s; metal oxidation $E_M = 0.5$ ($E_{pa} + E_{pc}$), V for Ru(III)/Ru(II) couple, $\Delta E_p = |E_{pa} - E_{pc}|$, mV; E_{pa} (anodic-peak-potential); E_{pc} (cathodic-peak-potential). E_L refers to ligand reduction.

$(CO)_2$(β-NaiPy)] (**1b**) have >40% contribution from Cl function and in *trans*-(I)-[$RuI_2(CO)_2$(β-NaiPy)] (**2b**) iodo contributes >70% to these MOs. The energy of HOMO of *trans*-(Cl)-[$RuCl_2(CO)_2$(β-NaiPy)] (**1b**) (E_{HOMO}, −6.08 eV; E_{HOMO-1}, −6.18 eV) is lower due to the higher electronegetivity of Cl than that of I in *trans*-(I)-[RuI_2-$(CO)_2$(β-NaiPy)] (**2b**) (E_{HOMO}, −5.83 eV; E_{HOMO-1}, −5.86 eV) (Figs. 3 and 4). Ruthenium orbitals contribute <35% in *trans*-(Cl)-[$RuCl_2$-$(CO)_2$(β-NaiPy)] (**1b**) and <25% in *trans*-(I)-[$RuI_2(CO)_2$(β-NaiPy)] (**2b**) to construct HOMO and HOMO-1 of the complexes. The lowest unoccupied MO, i.e. LUMO and also LUMO + 1, LUMO + 2 are characterized by β-NaiPy ligand orbitals (>90%) (Fig. 4). The transitions (>400 nm) in the complexes are admixture of metal-to-ligand and halide-to-ligand (XLCT) charge transferences (Table 4). *trans*-(I)-[$RuI_2(CO)_2$(β-NaiPy)] (**2b**) shows longer wavelength (546.5 nm) than *trans*-(I)-[$RuCl_2(CO)_2$(β-NaiPy)] (**1b**) (495.8 nm) that may be due to better electron donating ability of I than Cl. The transitions <400 nm are characterized as either intra-ligand charge transfer (ILCT where L = β-NaiPy), halide-ligand charge transfer (XLCT) or admixture of ILCT and XLCT. The TD-DFT calculation (Table 4) shows that the transition at wavelength >400 nm could be assigned to HOMO → LUMO/HOMO-1 → LUMO/HOMO − 1 → LUMO + 1.

Free ligands exhibit emission at 414 and 405 nm for α-NaiPy and β-NaiPy, respectively, at room temperature in $CHCl_3$ solution upon excitation at 330 nm [16]. The complexes, [$RuX_2(CO)_2$(Nai-Py)] (X = Cl, I) (**1**, **2**), exhibit intense emission upon excitation at 305–342 nm. The emission is assigned to π–π* state (Table 3). We do not observe any emission when the complexes are excited

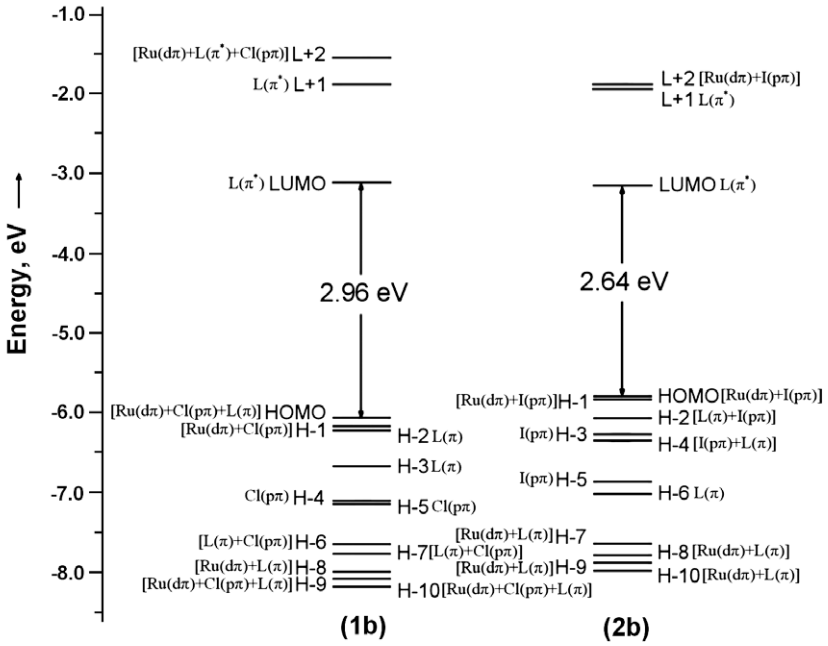

Fig. 3. Calculated orbital energy levels of *trans*-(I)-[$RuI_2(CO)_2$(β-NaiPy)] **(1b)** and *trans*-(Cl)-[$RuCl_2(CO)_2$(β-NaiPy)] (**2b**).

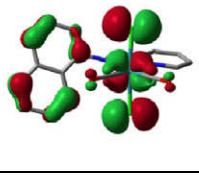	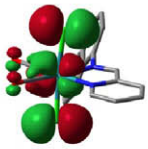	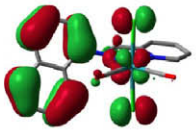	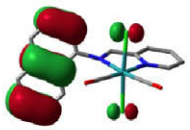
HOMO E = -6.08 eV; Ru, 32%; CO, 3%; L, 20%; Cl, 44%.	HOMO-1 E = -6.18 eV; Ru, 35%; Cl, 60%.	HOMO-2 E = -6.24 eV; Ru, 7%; CO, 3%; L, 79%; Cl, 13%.	HOMO-3 E = -6.69 eV; L, 95%; Cl, 5%.
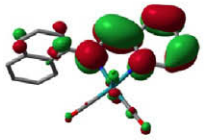		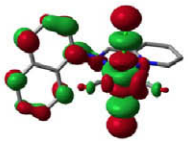	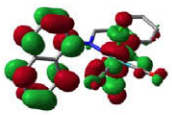
LUMO E = -3.12 eV; L, 95%	LUMO+1 E = -1.89 eV; L, 98%.	LUMO+2 E = -1.57 eV; Ru, 45%; CO, 6%; L, 27%; Cl, 22%.	LUMO+3 E = -1.34 eV; Ru, 25%; CO, 9%; L, 58%; Cl, 8%.

$[RuCl_2(CO)_2(\beta\text{-NaiPy})]$ (**1b**)

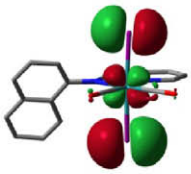	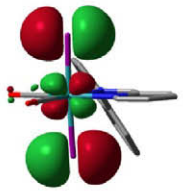	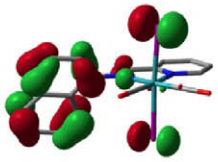	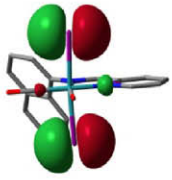
HOMO E = -5.83 eV; Ru, 24%; I, 73%.	HOMO-1 E = -5.86 eV; Ru, 22%; I, 76%.	HOMO-2 E = -6.10 eV; L, 72%; I, 27%.	HOMO-3 E = -6.31 eV; I, 95%.
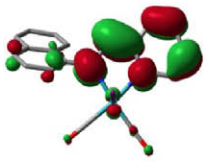	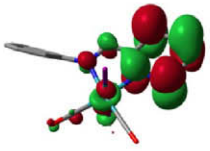	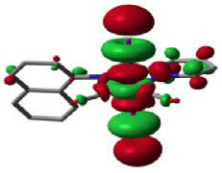	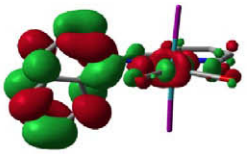
LUMO E = -3.19 eV; L, 92%.	LUMO+1 E = -1.98 eV; L, 90%.	LUMO+2 E = -1.94 eV; Ru, 43%; CO, 5%; L, 13%; I, 39%.	LUMO+3 E = -1.48 eV; Ru, 10%; CO, 5%; L, 84%.

$[RuI_2(CO)_2(\beta\text{-NaiPy})]$ (**2b**)

Fig. 4. Surface plot of the frontier orbitals of *trans*-(Cl)-$[RuCl_2(CO)_2(\beta\text{-NaiPy})]$ (**1b**) and *trans*-(I)-$[RuI_2(CO)_2(\beta\text{-NaiPy})]$ (**2b**).

at higher wavelength (>500 nm). We have taken π–π^* transition in the complexes to investigate emission properties (Fig. 2, Table 3). The quantum yields (ϕ) vary 0.006–0.08. The fluorescence quantum yield of the iodo complexes is lower than chloro complexes; this may be considered as heavy atom effect on fluorescence [38]. Again, $[RuX_2(CO)_2(\alpha\text{-NaiPy})]$ and $[RuX_2(CO)(MeCN)(\alpha\text{-NaiPy})]$ show higher quantum yield than $[RuX_2(CO)_2(\beta\text{-NaiPy})]$ and $[RuX_2(CO)(MeCN)(\beta\text{-NaiPy})]$. The quantum yields of the dicabonyl complexes (**1**, **2**) are higher than the corresponding monocarbonyl complexes (**3**, **4**) which may be due to the presence of additional π-acidic CO group. Because of π-acidity of CO the dd and MLCT transition energy raises even higher than ligand centered transition (ILCT) which reduces the radiationless decay process [21,39]. Thus CO coordination to Ru(II) may increase quantum yield.

Lifetime data of the complexes are taken at 298 K in acetonitrile solution when excited at 370 nm. The fluorescence decay curve was deconvoluted with respect to the lamp profile. The observed florescence decay fits with bi-exponential nature for the complexes (Fig. 5, Table 3). We have used mean fluorescence lifetime ($\tau_f = a_1\tau_1 + a_2\tau_2$ where a_1 and a_2 are relative amplitudes of decay process)

Table 4
Selected list of excited energies of [$RuCl_2(CO)_2$(β-NaiPy)] (**1b**) and [$RuI_2(CO)_2$(β-NaiPy)] (**2b**) in the acetonitrile phase.

Excitation energy (eV)	Wavelength, λ (nm)	Osc. strength (f)	Major contribution	Character
*[$RuCl_2(CO)_2$(β-NaiPy)] (**1b**) in acetonitrile*				
2.5004	495.8	0.0072	(95%)HOMO → LUMO	Ru(dπ)/Cl(pπ) → L(π*) (MLCT, XLCT)
2.5862	479.4	0.1076	(84%)HOMO − 1 → LUMO	Ru(dπ)/Cl(pπ) → L(π*) (MLCT, XLCT)
3.0564	405.6	0.0019	(74%)HOMO − 1 → LUMO + 1	Ru(dπ)/Cl(pπ) → L(π*), (MLCT, XLCT)
3.1850	389.5	0.0154	(45%)HOMO − 3 → LUMO	L(π) → L(π*) ILCT
			(39%)HOMO − 3 → LUMO + 1	
3.5488	349.4	0.1946	(72%)HOMO − 2 → LUMO + 3	L(π) → L(π*) ILCT
3.8564	321.5	0.0436	(55%)HOMO − 5 → LUMO	Cl(pπ) → L(π*) XLCT
			(38%)HOMO − 4 → LUMO	
4.0934	302.9	0.0873	(67%)HOMO − 3 → LUMO + 3	L(π) → L(π*) ILCT
4.3879	282.5	0.1091	(72%)HOMO − 7 → LUMO	Cl(pπ)/L(π) → L(π*) (XLCT, ILCT)
*[$RuI_2(CO)_2$(β-NaiPy)] (**2b**) in acetonitrile*				
2.2686	546.5	0.0065	(94%)HOMO → LUMO	Ru(dπ)/I(pπ) → L(π*) (MLCT, XLCT)
2.4859	498.7	0.0673	(83%)HOMO − 1 → LUMO	Ru(dπ)/I(pπ) → L(π*) (MLCT, XLCT)
2.8315	437.9	0.0065	(84%)HOMO → LUMO + 1	Ru(dπ)/I(pπ) → L(π*) (MLCT, XLCT)
3.0787	402.7	0.0129	(97%)HOMO − 2 → LUMO + 1	I(pπ)/L(π) → L(π*) (XLCT, ILCT)
3.7408	331.4	0.1675	(88%)HOMO − 6 → LUMO	L(π) → L(π*) (ILCT)
4.1183	301.0	0.0747	(72%)HOMO − 7 → LUMO	L(π) → L(π*) (ILCT)
4.1905	295.9	0.1257	(45%)HOMO − 6 → LUMO + 1	L(π) → L(π*) ILCT
			(24%)HOMO − 9 → LUMO	L(π) → L(π*) (ILCT)

X = Cl (**1b**)/I (**2b**).
MLCT: metal-to-ligand charge transfer; XLCT: halide (Cl or I)-to-ligand charge transfer; ILCT: intra-ligand charge transfer.

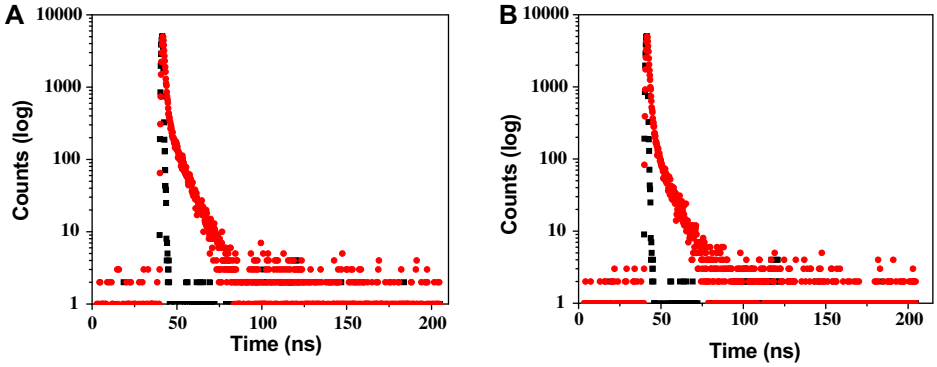

Fig. 5. Decay profile of *trans*-(Cl)-[$RuCl_2(CO)_2$(α-NaiPy)] (A) and *trans*-(Cl)-[$RuCl_2(CO)_2$(β-NaiPy)] (B).

to compare excited state stability of the complexes. The radiative and non-radiative rate constants (k_r and k_{nr}) are calculated and data show usual higher k_{nr} value than k_r (Table 3). The fluorescence lifetime of the complexes is in the range 0.8–1.3 ns. The fluorescence lifetime of the complexes is less than the ligands.

Photoirradiation of *trans*-(Cl)-[$RuCl_2(CO)_2$(β-NaiPy)] (**1b**) in MeCN solution shows spectral pattern of *trans*-(Cl)-[$RuCl_2$(CO)-(MeCN)(β-NaiPy)] and suggests replacement of a carbonyl by the solvent molecule [40]. The irradiation was continued until the original pair of ν(CO) bands in the IR spectrum was replaced by a single band at 1970 cm^{-1}. The product contained a mixture of two isomers with *ca.* 70% of the dominant component *trans*-(Cl)-[$RuCl_2$(CO)(CH_3CN)(β-NaiPy)]. It becomes difficult to unambiguous assignment of NMR of the mixed complexes due to large number of protons from coordinated ligands. Similar results of photoexcitation of *trans*-(Cl)-[$RuCl_2(CO)_2$(bpy)] supports this conjecture of CO substitution by MeCN [40].

3.3.3. ^1H NMR spectra

The ^1H NMR spectra were assigned on comparing with free ligand values and reported complexes [16,17]. The spectra are recorded in DMSO-d_6 solution (Table 5). Important observation is the downfield shifting of pyridine protons (3- to 6-H) by 0.2–0.5 ppm. This supports the coordination of pyridine-N to metal center. Naphthyl protons (8-H to 15-H) experience small perturbation and the chemical shift data are comparable with free ligand data. Imine proton (–CH=N–) appears as a singlet at 8.5–8.7 ppm (Table 5). The complexes **3**, **4** show a singlet around 2.06–2.07 ppm, which supports the presence of CH_3CN in these complexes.

3.3.4. Electrochemistry

The electrochemical behavior of the complexes was investigated by cyclic voltammetry (CV) in presence of [NBu_4][ClO_4] in MeCN at scan rate 50 mV S^{-1}. The compounds show one oxidative response positive to reference electrode and one reduction negative to this reference (Ag/AgCl) in the potential range 2.0 to −2.0 V (Table 3). Reduction is irreversible in nature as evident from peak-to-peak separation (ΔE_p > 170 mV) (Fig. 6). One single electron oxidation is also irreversible in the range of 1.3–1.5 V for **1** and **2**; 0.8–0.9 V for **3** and **4** and is assigned to Ru(III)/Ru(II) couple. DFT calculation of **1b** and **2b** show that the HOMO has halide contribution (44% in **1b** and 73% in **2b**) and thus the oxidation may be referred to oxidation of X^- to $1/2X_2$ those may inherently oxidize Ru(II) → Ru(III). Thus the process follows classical EC mechanism [41]. Iodo complexes, [$RuI_2(CO)_2$(NaiPy)] (**2**) exhibit lower potential (1.3 V for **2** and 0.8 V for **4**) than chloro derivatives, [$RuCl_2(CO)_2$(NaiPy)] (1.5 V for **1** and 0.9 V for **3**) which may be

Table 5
^{1}H NMR spectral data of the complexes (**1**-**4**) in DMSO-d_6.

Compound	δ (ppm)									
	3-H[a]	4-H[b]	5-H[b]	6-H[a]	7-H[c]	8-H[a]	9-H[a]	10-H[a]	11-H-14-H[d]	15-H[a]
$[RuCl_2(CO)_2(\alpha\text{-NaiPy})]$ (**1a**)	8.06 (9.0)	8.18 (9.0)	8.18 (9.0)	8.43 (9.0)	8.67		7.95	7.80 (9.0)	7.59	7.46 (9.0)
$[RuCl_2(CO)_2(\beta\text{-NaiPy})]$ (**1b**)	7.96 (9.0)	7.91 (9.0)	7.91 (9.0)	8.32 (9.0)	8.63	7.82 (9.0)		7.68 (9.0)	7.58	7.31 (9.0)
$[RuI_2(CO)_2(\alpha\text{-NaiPy})]$ (**2a**)	8.03 (9.0)	7.98 (9.0)	7.98 (9.0)	8.15 (9.0)	8.63		7.90 (9.0)	7.84 (9.0)	7.54	6.80 (9.0)
$[RuI_2(CO)_2(\beta\text{-NaiPy})]$ (**2b**)	8.00 (9.0)	7.92 (9.0)	7.92 (9.0)	8.10 (9.0)	8.60	7.82 (9.0)		7.74 (7.5)	7.56	6.76 (9.0)
$[RuCl_2(CO)(CH_3CN)(\alpha\text{-NaiPy})]$ (**3a**)	8.00 (9.0)	7.93 (9.0)	7.93 (9.0)	8.40 (9.0)	8.51		7.85 (9.0)	7.83 (9.0)	7.56	7.52 (9.0)
$[RuCl_2(CO)(CH_3CN)(\beta\text{-NaiPy})]$ (**3b**)	7.95 (9.0)	7.90 (9.0)	7.90 (9.0)	8.28 (9.0)	8.48	7.78 (9.0)		7.83 (9.0)	7.57	7.36 (9.0)
$[RuI_2(CO)(CH_3CN)(\alpha\text{-NaiPy})]$ (**4a**)	7.92 (9.0)	7.88 (9.0)	7.88 (9.0)	8.30 (9.0)	8.46		7.80 (9.0)	7.77 (9.0)	7.50	7.40 (9.0)
$[RuI_2(CO)(CH_3CN)(\beta\text{-NaiPy})]$ (**4b**)	7.90 (9.0)	7.83 (9.0)	7.83 (9.0)	8.25 (9.0)	8.50	7.81 (9.0)		7.72 (9.0)	7.52	7.34 (9.0)

[a] Doublet.
[b] Triplet.
[c] Singlet.
[d] Multiplet.

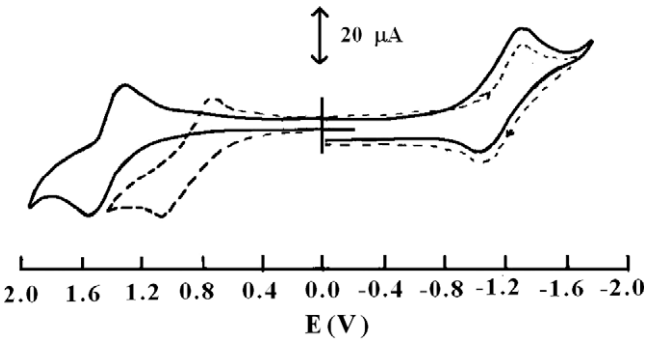

Fig. 6. Cyclic voltammogram of **1b** (–) and **3b** (- -) in MeCN using Pt-disk working and Pt-wire auxiliary electrodes and reference to Ag/AgCl electrode.

due to higher electronegativity of Cl than I. Energy of HOMO by DFT (Fig. 3) also explains this observation: the E_{HOMO} (−6.08 eV) of **1b** is lower than **2b** (−5.83 eV). The one electron nature of the oxidation has been confirmed by comparing its current height with that of the standard ferrocene/ferrocenium couple under identical experimental conditions. On the other hand the one reductive responses can be attributed to the reduction of the diimine ligand which can accommodate the electrons to its π^* MO. The DFT data have assigned that the LUMO of the complexes are constituted mainly by imine group of ligand (>90%) and thus the reduction is considered as electron accommodation at imine dominated orbitals.

4. Conclusion

We synthesized and characterized *trans*-(X)-$[RuX_2(CO)_2$-(α/β-NaiPy)] (α/β-NaiPy = N-[(2-pyridyl)methyliden]-α(or β)-aminonaphthalene) (X = Cl, I). In one case the structure has been confirmed by single crystal X-ray diffraction study. *trans*-(X)-$[RuX_2(CO)(MeCN)(\alpha/\beta\text{-NaiPy})]$ are synthesized by reacting Me_3NO with dicarbonyl precursor. All the complexes are redox active and possess good fluorescence property. The optimized geometries, frequencies, energies, frontier orbitals and excited states that emerged from DFT to TD-DFT calculations provided a detailed description of the spectra and redox properties of the complexes.

Acknowledgements

Financial support from Department of Science & Technology and University Grants Commission, New Delhi are gratefully acknowledged. One of us (P.D.) thanks to the Council of Scientific and Industrial Research, New Delhi for fellowship.

Appendix A. Supplementary material

CCDC 697916 contains the supplementary crystallographic data for this paper. These data can be obtained free of charge from The Cambridge Crystallographic Data Centre via www.ccdc.cam.ac.uk/data_request/cif.

Supplementary data associated with this article can be found, in the online version, at doi:10.1016/j.jorganchem.2009.09.017.

References

[1] (a) J. Reedijk, in: G. Willkinson, J.A. McCleverty (Eds.), Comprehensive Coordination Chemistry, vol. 2, Pergamon, Oxford, UK, 1987, p. 430;
(b) W.T. Wong, Coord. Chem. Rev. 131 (1994) 45;
G. Wilkinson, F.G.A. Stone, E.W. Abel (Eds.), Comprehensive Organometallic Chemistry, Pergamon Press, New York, 1982;
(c) F.A. Cotton, G. Wilkinson, Advanced Inorganic Chemistry, fifth ed., Wiley-Intersciences, New York, 1994.
[2] (a) C. Kaes, A. Katz, M.W. Hasseini, Chem. Rev. 100 (2000) 3553;
(b) M. Venturi, A. Credi, V. Balzani, Coord. Chem. Rev. 186 (1999) 233.
[3] (a) C. Piguet, G. Bernardinelli, G. Hopfgartner, Chem. Rev. 97 (1997) 2005;
(b) U. Knof, A. von Zelewsky, Angew. Chem., Int. Ed. 38 (1999) 303;
(c) K. Kalyanasundaram, M. Grätzel, Coord. Chem. Rev. 347 (1998);
V. Balzani, A. Juris, M. Venturi, S. Campagna, S. Serroni, Chem. Rev. 96 (1996) 759.
[4] M. Gratzel, Energy Resources through Photochemistry and Catalysis, Academic, New York, 1983.
[5] E.N. Tokel-Takvoryan, E.R. Hemingway, A.J. Bard, J. Am. Chem. Soc. 95 (1973) 6582.
[6] (a) M.R. Hartshorn, K.J. Barton, J. Am. Chem. Soc. 114 (1992) 5919;
(b) L. Sacksteder, M. Lee, J.N. Demas, B.A. DeGraff, J. Am. Chem. Soc. 115 (1993) 8230.
[7] (a) B.K. Ghosh, A. Chakravorty, Coord. Chem. Rev. 95 (1989) 239;
(b) N. Bag, A. Pramanik, G.K. Lahiri, A. Chakravorty, Inorg. Chem. 31 (1992) 40;
(c) R.E. Shepherd, Coord. Chem. Rev. 247 (2002) 147;
(d) C.G. Hotze, H. Kooijman, A.L. Spek, J.G. Haasnoot, J. Reedijk, New J. Chem. 28 (2004) 565;
(e) M.J. Overett, J.R. Moss, Inorg. Chim Acta 358 (2005) 1715.
[8] (a) A.B. Moyer, S.M. Thompson, T.J. Meyer, J. Am. Chem. Soc. 102 (1980) 2310;
(b) S.M. Thompson, T.J. Meyer, J. Am. Chem. Soc. 103 (1981) 5577;
(c) T.J. Meyer, J. Electrochem. Soc. 131 (1984) 221C.
[9] (a) B.P. Sullivan, D.J. Salmon, T.J. Meyer, Inorg. Chem. 17 (1978) 3334;
(b) M.M.R. Bruce, E. Megebee, B.P. Sullivan, H.H. Thorp, R.T. O'Toole, A. Downard, R.J. Pugh, T.J. Meyer, Inorg. Chem. 31 (1992) 4864.
[10] E.C. Constable, Coord. Chem. Rev. 93 (1989) 205.
[11] (a) L.A. Garcia-Escudero, D. Miguel, J.A. Turiel, J. Organomet. Chem. 691 (2006) 3434;
(b) M. Menon, A. Pramanik, A. Chakravorty, Inorg. Chem. 34 (1995) 3310;
A. Mentes, Transition Met. Chem. 24 (1999) 77.
[12] E.C. Fitzgerald, R.W. Grime, H.C. Knight, M. Helliwell, J. Raftery, M.W. Whiteley, J. Organomet. Chem. 691 (2006) 1879.
[13] (a) J.M. Kelly, J.G. Vos, Angew Chem., Int. Ed. Engl. 21 (1982) 628;
(b) J.G. Hassnoot, W. Hinrichs, O. Weir, J.G. Vos, Inorg. Chem. 25 (1986) 4140;
(c) H. Ishida, K. Tanaka, M. Moromoto, T. Tanaka, Organometallics 5 (1986) 724;
(d) L. Alvila, T.A. Pakkanen, O. Krause, J. Mol. Catal. 84 (1993) 145. and references therein.
[14] (a) J.-M. Lehn, R. Ziesel, J. Organomet. Chem. 382 (1990) 157;
(b) M. Ishida, K. Fujiki, T. Omba, K. Ohkubo, K. Tanaka, T. Terarda, T. Tanaka, J. Chem. Soc., Dalton Trans. (1990) 2155.

[15] (a) A. Sandouka, B.J. Fuller, B.E. Mann, C.J. Green, R. Foresti, R. Motterlini, Kidney Int. 69 (2006) 239;
(b) P. Sawle, J. Hammad, I.J.S. Fairlamb, B. Moulton, C.T. O'Brien, J.M. Lynam, A.K. Duhme-Klair, R. Foresti, R. Motterlini, J. Pharma. Exp. Therapeut. 318 (2006) 403.
[16] (a) J. Dinda, C. Sinha, Transition Met. Chem. 28 (2003) 864;
(b) P. Datta, C. Sinha, Polyhedron 26 (2007) 2433.
[17] (a) D. Das, J. Dinda, T.K. Mondal, C. Sinha, J. Indian Chem. Soc. 83 (2006) 342;
(b) D. Das, B.G. Chand, K.K. Sarker, J. Dinda, C. Sinha, Polyhedron 25 (2006) 2333;
(c) D. Das, B.G. Chand, J. Dinda, C. Sinha, Polyhedron 26 (2007) 555.
[18] J. Zhang, W. Li, W. Bu, L. Wu, L. Ye, G. Yang, Inorg. Chim. Acta 358 (2005) 964.
[19] L.G. Nickolacheva, C.M. Vogels, R.A. Stefan, H.A. Warwish, S.J. Duffy, R.J. Ireland, A. Decken, R.H. Hudson, S.A. Westcott, Canadian J. Chem. 81 (2003) 269.
[20] (a) M.I. Bruce, Ruthenium carbonyls and related compounds, in: G. Wilkinson, F.G.A. Stone, E.W. Abel (Eds.), Comprehensive Organometallic Chemistry, vol. 4, Pergamon Press, Oxford, 1982, p. 661;
(b) A.J. Deeming, C. Forth, G. Hogarth, Transition Met. Chem. 31 (2006) 42;
(c) M. Haukka, J. Kiviaho, M. Ahlgren, T.A. Pakkam, Organometallics 14 (1995) 825.
[21] (a) D.V. O'Connor, D. Phillips, Time Correlated Single Photon Counting, Academic Press, New York, 1984;
(b) B. Valuer, Molecular Fluorescence: Principles and Applications, Wiley-VCH, Weinheim, 2001.
[22] Bruker, SMART and SAINT, Bruker AXS Inc., Madison, WI, USA, 1998.
[23] G.M. Sheldrick, SHELXS 97, "Program for the Solution of Crystal Structure", University of Gottingen, Germany, 1997.
[24] G.M. Sheldrick, SHELXL 97, "Program for the Solution of Crystal Structure", University of Gottingen, Germany, 1997.
[25] A.L. Spek, PLATON "Molecular Geometry Program", University of Utrecht, The Netherlands, 1999.
[26] L.J. Farrugia, J. Appl. Cryst. 30 (1997) 565.
[27] C. Lee, W. Yang, R.G. Parr, Phys. Rev. B 37 (1988) 785.
[28] D. Andrae, U. Haeussermann, M. Dolg, H. Stoll, H. Preuss, Theor. Chim. Acta 77 (1990) 123;
P. Fuentealba, H. Preuss, H. Stoll, L.V. Szentpaly, Chem. Phys. Lett. 89 (1989) 418.
[29] M.J. Frisch, G.W. Trucks, H.B. Schlegel, G.E. Scuseria, M.A. Robb, J.R. Cheeseman, J.A. Montgomery Jr., T. Vreven, K.N. Kudin, J.C. Burant, J.M. Millam, S.S. Iyengar, J. Tomasi, V. Barone, B. Mennucci, M. Cossi, G. Scalmani, N. Rega, G.A. Petersson, H. Nakatsuji, M. Hada, M. Ehara, K. Toyota, R. Fukuda, J. Hasegawa, M. Ishida, T. Nakajima, Y. Honda, O. Kitao, H. Nakai, M. Klene, X. Li, J.E. Knox, H.P. Hratchian, J.B. Cross, V. Bakken, C. Adamo, J. Jaramillo, R. Gomperts, R.E. Stratmann, O. Yazyev, A.J. Austin, R. Cammi, C. Pomelli, J.W. Ochterski, P.Y. Ayala, K. Morokuma, G.A. Voth, P. Salvador, J.J. Dannenberg, V.G. Zakrzewski, S. Dapprich, A.D. Daniels, M.C. Strain, O. Farkas, D.K. Malick, A.D. Rabuck, K. Raghavachari, J.B. Foresman, J.V. Ortiz, Q. Cui, A.G. Baboul, S. Clifford, J. Cioslowski, B.B. Stefanov, G. Liu, A. Liashenko, P. Piskorz, I. Komaromi, R.L. Martin, D.J. Fox, T. Keith, M.A. Al-Laham, C.Y. Peng, A. Nanayakkara, M. Challacombe, P.M.W. Gill, B. Johnson, W. Chen, M.W. Wong, C. Gonzalez, J.A. Pople, Gaussian Inc., Wallingford CT, 2004.
[30] GAUSSVIEW3.0, Gaussian, Pittsburgh, PA.
[31] R. Bauernschmitt, R. Ahlrichs, Chem. Phys. Lett. 256 (1996) 454;
R.E. Stratmann, G.E. Scuseria, M.J. Frisch, J. Chem. Phys. 109 (1998) 8218;
M.E. Casida, C. Jamorski, K.C. Casida, D.R. Salahub, J. Chem. Phys. 108 (1998) 4439.
[32] V. Barone, M. Cossi, J. Phys. Chem. A 102 (1998) 1995;
M. Cossi, V. Barone, J. Chem. Phys. 115 (2001) 4708;
M. Cossi, N. Rega, G. Scalmani, V. Barone, J. Comput. Chem. 24 (2003) 669.
[33] N.M. O'Boyle, A.L. Tenderholt, K.M. Langner, J. Comput. Chem. 29 (2008) 839.
[34] M. Haukka, J. Kiviaho, M. Ahlgrén, T.A. Pakkanen, Organometallics 14 (1995) 825;
S. Luukkanen, M. Haukka, O. Laine, T. Venäläinen, P. Vainiotalo, T.A. Pakkanen, Inorg. Chim. Acta 332 (2002) 25.
[35] (a) T.K. Mondal, S.K. Sarker, P. Raghavaiah, C. Sinha, Polyhedron 27 (2008) 3020;
(b) T.K. Mondal, J. Dinda, J. Cheng, T.-H. Lu, C. Sinha, Inorg. Chim. Acta 361 (2008) 2431.
[36] (a) E.Y. Li, Y.-M. Cheng, C.-C. Hsu, P.-T. Chou, G.-S. Lee, I.-H. Lin, Y. Chi, C.-S. Liu, Inorg. Chem. 45 (2006) 8041;
(b) E. Eskelinen, M. Haukka, T. Venalainen, T.A. Pakkanen, M. Wasberg, S. Chardon-Noblat, A. Deronzier, Organometallics 19 (2000) 163.
[37] R.A. Krause, K. Krause, Inorg. Chem. 23 (1984) 2195.
[38] J.L. Klappa, A.A. Geers, S.J. Schmidtke, L.A. MacManus-Spencer, K. McNeill, Dalton Trans. (2004) 883.
[39] (a) P.A. Anderson, F.R. Keene, T.J. Meyer, J.A. Moss, G.F. Strouse, J.A. Treadway, J. Chem. Soc., Dalton Trans. (2002) 3820;
(b) E.Y. Li, Y.-M. Cheng, C.-C. Hsu, Pi.T. Chou, G.-H. Lee, I.-H. Lin, Y. Chi, C.-S. Liu, Inorg. Chem. 45 (2006) 8041.
[40] N.C. Fletcher, F.R. Keene, J. Chem. Soc., Dalton Trans. (14) (1998) 2293.
[41] C.-D. Sauthier, M. Noelle, D. Alain, Z. Raymond, J. Electroanal. Chem. 350 (1993) 43.